Supporting Information

Mo-doped SnS_2 with enriched S-vacancies for highly efficient electrocatalytic N_2 reduction: the critical role of Mo-Sn-Sn trimer

Ke Chu*, Jing Wang, Ya-ping Liu, Qing-qing Li, Ya-li Guo

School of Materials Science and Engineering, Lanzhou Jiaotong University, Lanzhou 730070, China

*Corresponding author. E-mail address: chukelut@163.com (K. Chu)

Experimental

Synthesis of Mo-SnS_2/CC

All the chemicals were used as received without further purification. In brief, a piece of carbon cloth (CC, 2 cm × 4 cm) was ultrasonically treated in concentrated HCl for 2 h, and cleaned with ethanol and distilled water several times. Then, 0.18 mM of thioacetamide and 0.09 mM of $SnCl_4 \cdot 5H_2O$ were dissolved in 30 mL of deionized water under stirring for 10 min, followed by addition of 0.001 mM of $(NH_4)_6Mo_7O_{24} \cdot 4H_2O$ under stirring for another 10 min. The mixed solution was transferred into a Teflon-lined stainless-steel autoclave, followed by immersing the pretreated CC in the solution. The autoclave was sealed and maintained at 180 ^{o}C for 24 h. After cooling to room temperature, the obtained Mo-SnS_2/CC was washed with deionized water and ethanol several times, and dried at 60 ^{o}C overnight. For comparison, the pristine SnS_2/CC was prepared by the same procedure without addition of $(NH_4)_6Mo_7O_{24} \cdot 4H_2O$.

Electrochemical measurements

Electrochemical measurements were tested on a CHI-660E electrochemical workstation in a three-electrode configuration including working electrode (CC sample), reference electrode (Ag/AgCl), and counter electrode (graphite rod). All potentials were referenced to the reversible hydrogen electrode (RHE). The RHE calibration was experimentally conducted in the high-purity hydrogen saturated 0.5 M $LiClO_4$ electrolyte by cyclic voltammeters curves, with using graphite rod and Pt wire as counter and working electrodes, respectively (Fig. S2). The NRR tests were conducted in an H-type two-compartment electrochemical cell separated by a Nafion 211 membrane. An absorber was set at the end of cell to avoid the loss of produced NH_3 by N_2 flow. The Nafion membrane was pretreated by boiling it in 5% H_2O_2 solution for 1 h, 0.5 M H_2SO_4 for 1 h and deionized water for 1 h in turn. During each electrolysis, ultra-high-purity N_2 gas (99.999%) was continuously purged into the cathodic chamber at a flow rate of 20 mL min^{-1}. After each NRR electrolysis, the solution in absorber was poured back into the cathodic compartment for the NH_3

detection. The produced NH_3 and possible N_2H_4 were quantitatively determined by the indophenol blue method[1], and approach of Watt and Chrisp[2], respectively.

Determination of NH_3

Typically, 4 mL of electrolyte was removed from the electrochemical reaction vessel. Then 50 μL of solution containing NaOH (0.75 M) and NaClO (ρ_{Cl} = ~4.5), 500 μL of solution containing 0.32 M NaOH, 0.4 M $C_7H_6O_3Na$, and 50 μL of $C_5FeN_6Na_2O$ solution (1 wt%) were respectively added into the electrolyte. After standing for 2 h, the UV-Vis absorption spectrum was measured and the concentration-absorbance curves were calibrated by the standard NH_4Cl solution with a serious of concentrations.

NH_3 yield was calculated by the following equation:

$$NH_3 \text{ yield } (\mu g \text{ h}^{-1} \text{ mg}_{\text{cat.}}^{-1}) = \frac{c_{NH_3} \times V}{t \times m} \quad (1)$$

Faradaic efficiency was calculated by the following equation:

$$\text{Faradaic efficiency } (\%) = \frac{3 \times F \times c_{NH_3} \times V}{17 \times Q} \times 100\% \quad (2)$$

where c_{NH3} (μg mL^{-1}) is the measured NH_3 concentration, V (mL) is the volume of the electrolyte, t (h) is the reduction time and m (mg) is the mass loading of the catalyst on CC. F (96500 C mol^{-1}) is the Faraday constant, Q (C) is the quantity of applied electricity.

Determination of N_2H_4

Typically, 5 mL of electrolyte was removed from the electrochemical reaction vessel. The 330 mL of color reagent containing 300 mL of ethyl alcohol, 5.99 g of $C_9H_{11}NO$ and 30 mL of HCl were prepared, and 5 mL of color reagent was added into the electrolyte. After stirring for 10 min, the UV-vis absorption spectrum was measured and the concentration-absorbance curves were calibrated by the standard N_2H_4 solution with a serious of concentrations.

Characterizations

X-ray diffraction (XRD) pattern was recorded on a Rigaku D/max 2400 diffractometer. X-ray photoelectron spectroscopy (XPS) analysis

was performed on a PHI 5702 spectrometer. Scanning electron microscopy (SEM) was carried out on a JSM-6701 microscope. Transmission electron microscopy (TEM), high-resolution transmission electron microscopy (HRTEM), and high-angle annular dark field (HAADF)-scanning transmission electron microscopy (STEM) were performed on a Tecnai G^2 F20 microscope. Electron paramagnetic resonance (EPR) measurements were performed on a Bruker ESP-300 spectrometer. Ion chromatogram measurements were conducted on a Dionex ICS-2000 ion chromatographs. ^1H nuclear magnetic resonance (NRM) measurements were performed on a 500 MHz Bruker superconducting-magnet NMR spectrometer. Prior to NMR measurements, $^{14}N_2$ or $^{15}N_2$ feed gas was purified by an acid trap (0.05 M H_2SO_4) to eliminate the potential NO_x and NH_3 contaminants.

Calculation details

Spin-polarized density functional theory (DFT) calculations were performed using Cambridge sequential total energy package (CASTEP)[3]. The Perdew−Burke−Ernzerh of (PBE) of generalized gradient approximation (GGA) was used for the exchange-correlation potential. DFT-D method was employed to calculate the van der Waals (vdW) interaction. A Gamma-point centered 3×3×1 k-mesh was adopted for structural optimizations, and a plane wave cutoff was set to 500 eV. Energy and force was not reach convergence until lower to 1×10^{-5} eV and 0.02 eV/Å, respectively. SnS_2 (001) was modeled by a 4×4 supercell, and a vacuum space of around 15 Å was set along the z direction to avoid the interaction between periodical images.

The computational hydrogen electrode (CHE) model was used to calculate the Gibbs free energy change (ΔG) of reaction steps:

$$\Delta G=\Delta E+\Delta ZPE-T\Delta S+\Delta G_{\mathrm{U}}+\Delta G_{\mathrm{pH}} \quad (3)$$

where ΔE is the electronic energy difference, ΔZPE is the zero point energy difference, T is the room temperature (298 K) and ΔS is the entropy change. ΔG_{U} is the contribution of electrode potential, which can be calculated by: $\Delta G_{\mathrm{U}} = -eU$, where and U is the applied potential. ΔG_{pH} is the free energy correction of pH, which can be

calculated by: $\Delta G_{pH} = -k_B T \times pH \times \ln 10$, where k_B is the Boltzmann constant, and the value of pH was set to be 7 for neutral medium used in our work. The transition state of water dissociation was analyzed by a combined linear synchronous transit (LST) and quadratic synchronous transit (QST) tools.

The formation energy (E_f) of SnS_2 containing Mo-dopant and V_s (Mo-SnS_2-V_s) can be calculated as:

$$E_f(\text{Mo-SnS}_2\text{-V}_s) = E(\text{Mo-SnS}_2\text{-V}_s) - E(\text{SnS}_2) - \mu_{Mo} + \mu_{Sn} + \mu_s \quad (4)$$

where E is the total energies of corresponding structures, μ is the chemical potential of corresponding atoms.

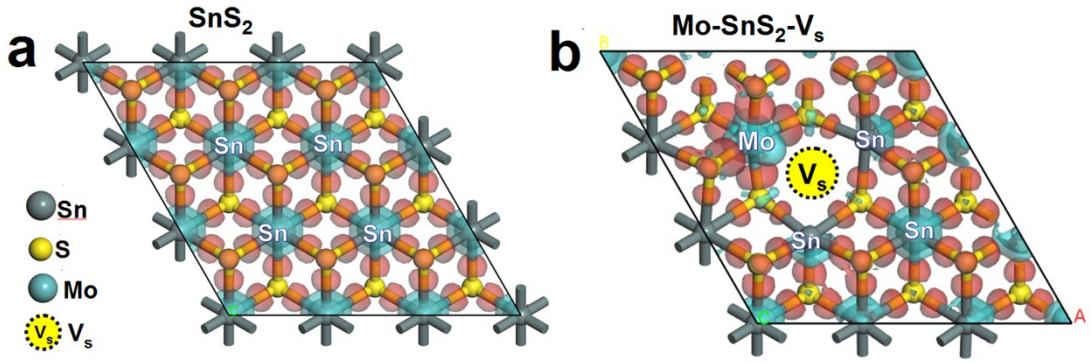

Fig. S1. Charge density distributions of (a) pristine SnS_2 and (b) Mo-SnS_2-V_s. Red and cyan regions correspond to the electron accumulation and depletion, respectively.

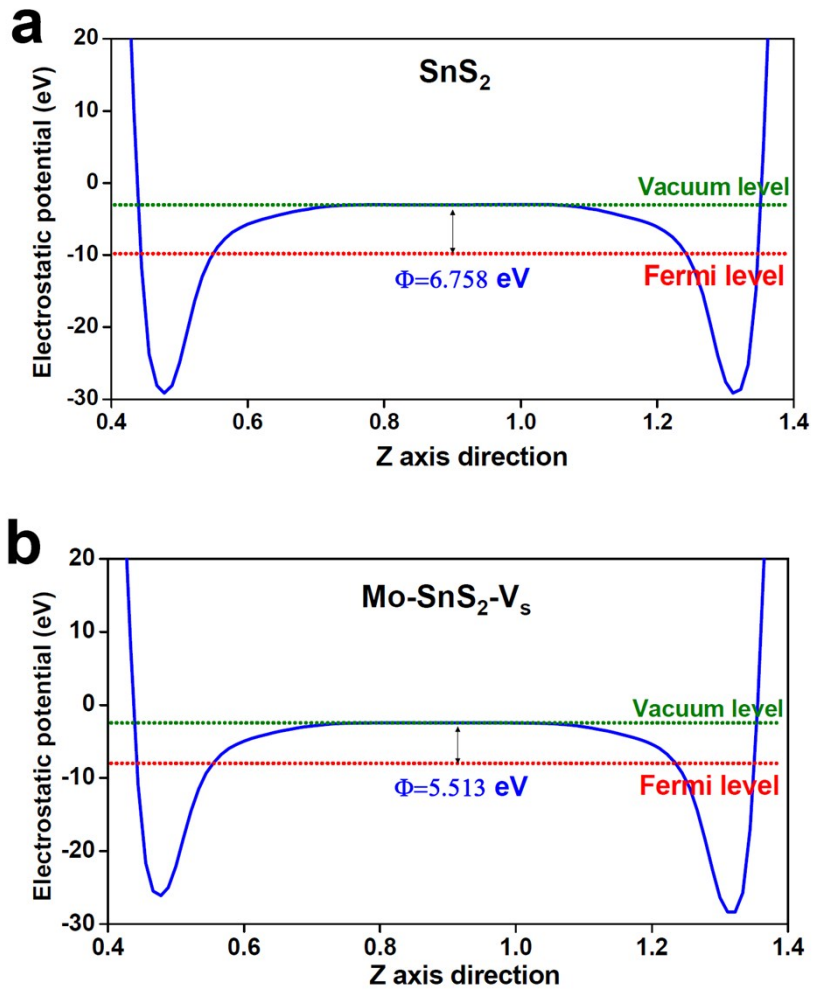

Fig. S2. Average potential profiles along c-axis direction for calculating the work functions of (a) SnS_2 and (b) Mo-SnS_2-V_s.

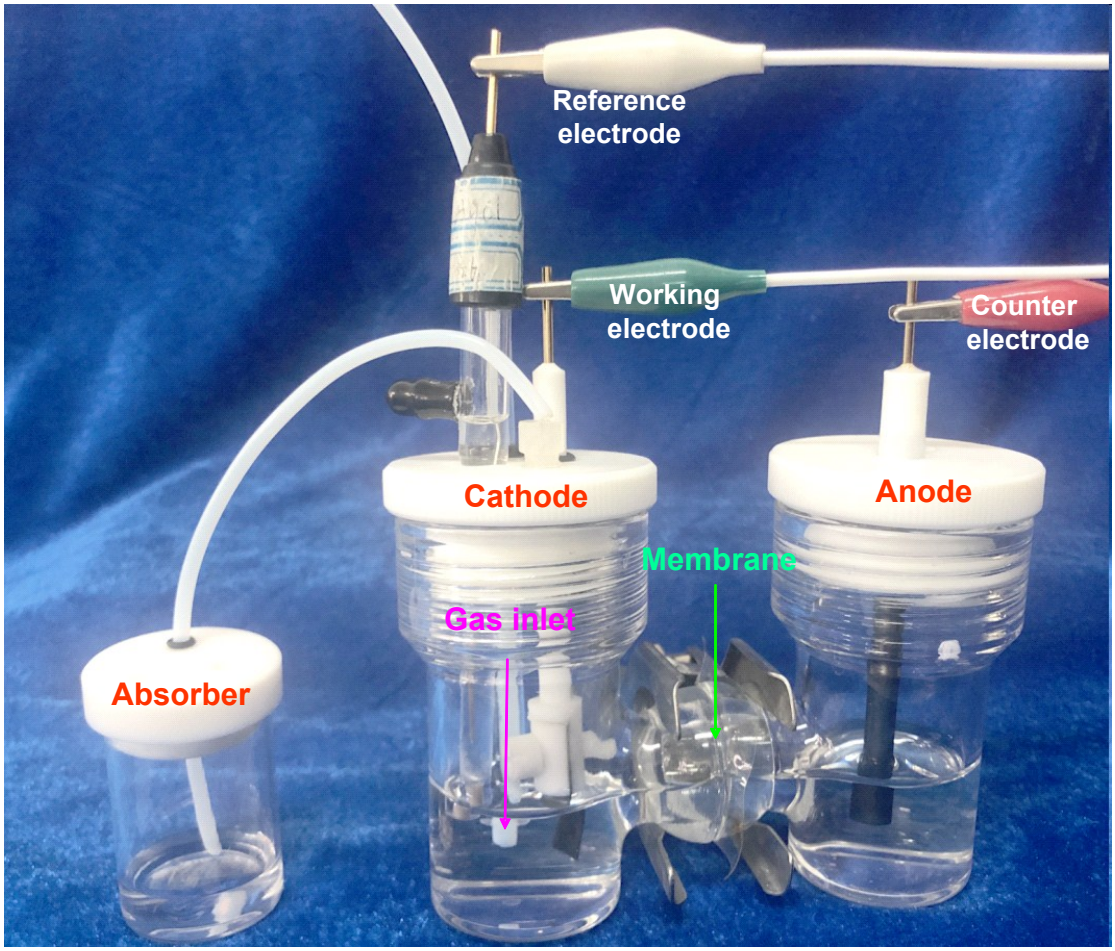

Fig. S3. Photograph of H-type electrochemical setup.

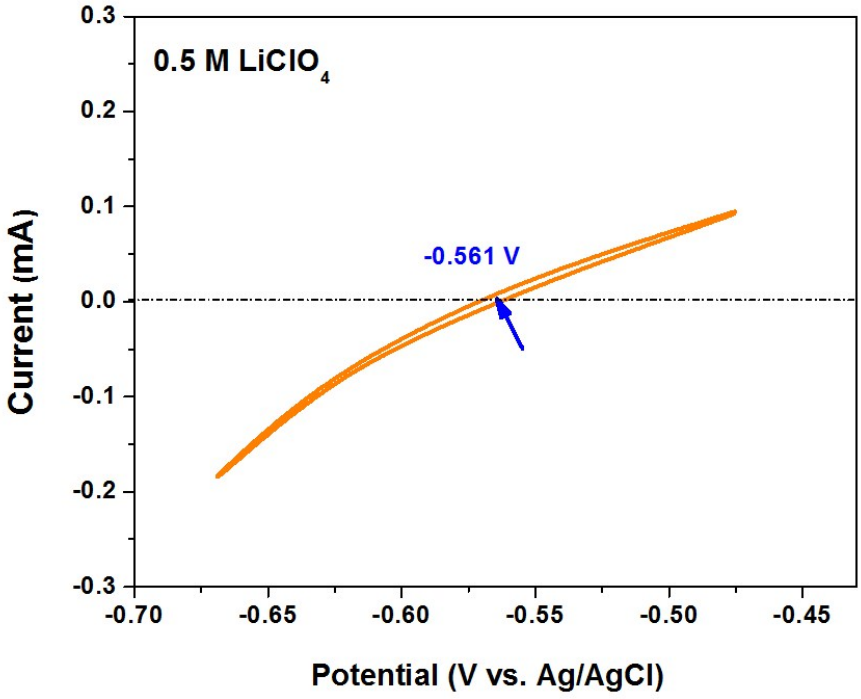

Fig. S4. The RHE calibration in 0.5 M $LiClO_4$ electrolyte.

The RHE calibration was conducted in the high-purity hydrogen saturated 0.5 M $LiClO_4$ electrolyte. The graphite rod and Pt wire were used as the counter and working electrodes, respectively. The cyclic voltammetry curves were performed at a scan rate of 1 mV s^{-1}. The RHE calibration potential for the hydrogen oxidation/evolution reactions is the average value of the two potentials at which the current crosses zero. It is shown in Fig. S4 that the *E*(RHE) is larger than *E*(Ag/AgCl) by 0.561 V. Therefore, we have *E*(RHE) = *E*(Ag/AgCl) +0.561.

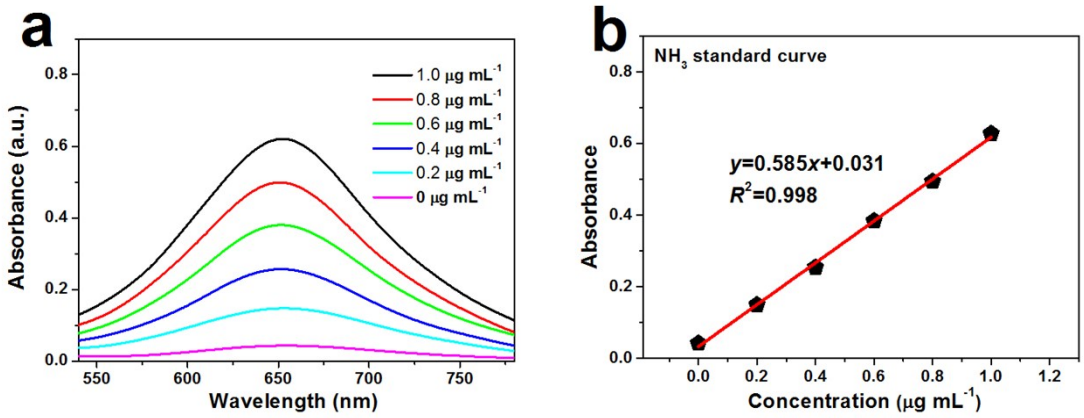

Fig. S5. (a) UV-Vis absorption spectra of indophenol assays with NH_4Cl after incubated for 2 h at ambient conditions. (b) Calibration curve used for calculation of NH_3 concentrations.

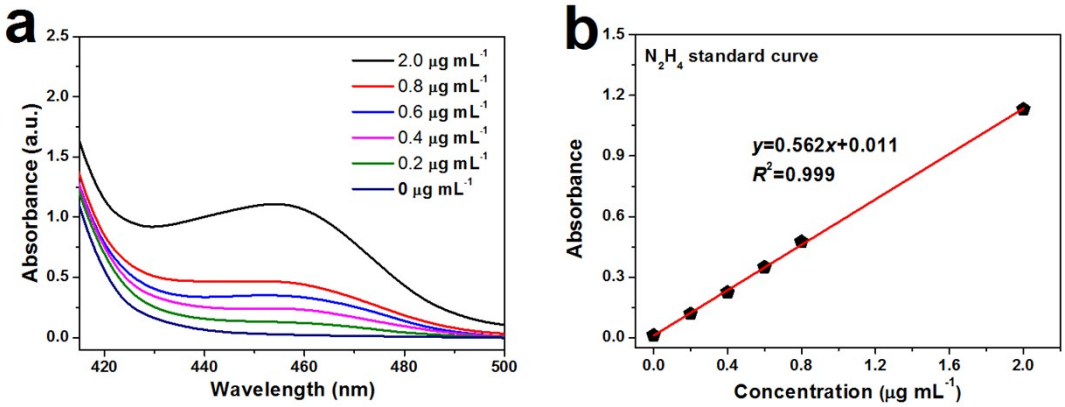

Fig. S6. (a) UV-Vis absorption spectra of N_2H_4 assays after incubated for 20 min at ambient conditions. (b) Calibration curve used for calculation of N_2H_4 concentrations.

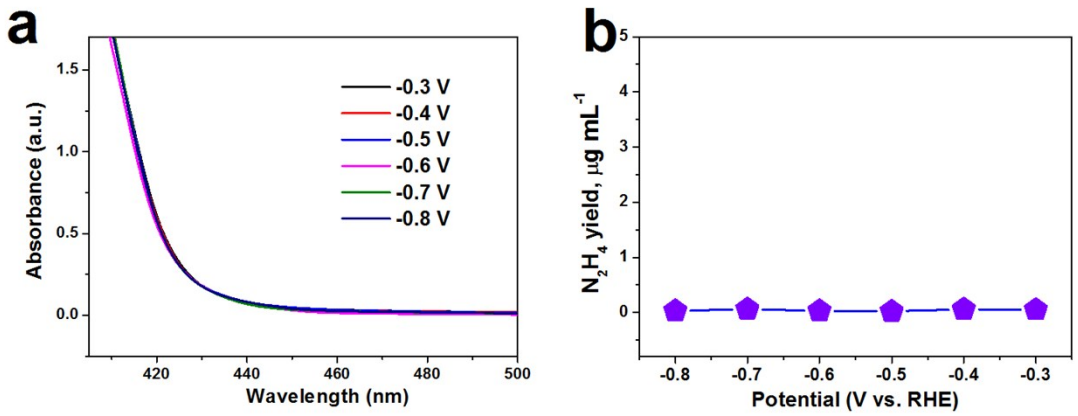

Fig. S7. (a) UV-Vis spectra of the electrolytes (stained with the chemical indicator based on the method of Watt and Chrisp) after 2 h electrocatalysis on Mo-SnS_2/CC at various potentials, and (b) corresponding N_2H_4 concentrations in the electrolytes.

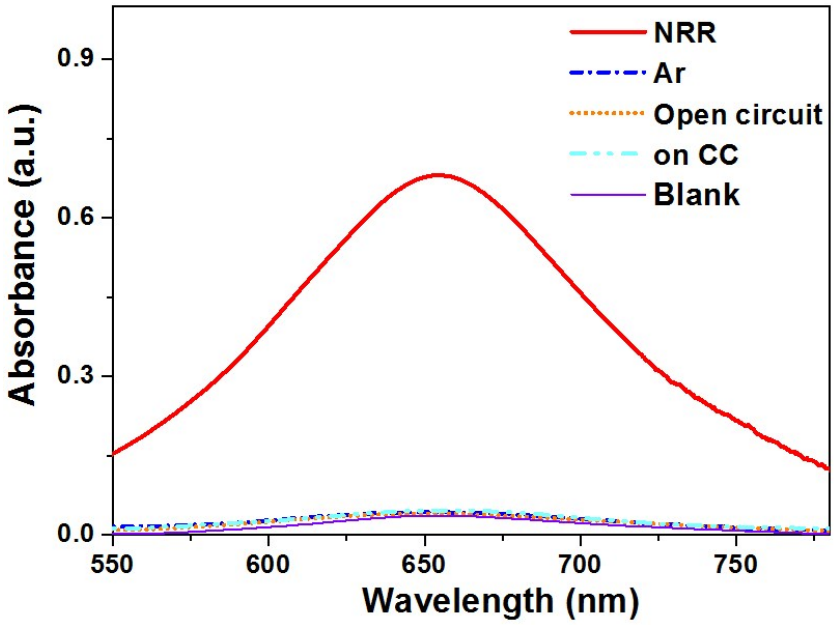

Fig. S8. UV-Vis absorption spectra of working electrolytes after 2 h of electrolysis on Mo-SnS_2/CC at -0.5 V in N_2-saturated solution, Ar-saturated solutions, N_2-saturated solution at open circuit, N_2-saturated solution on pristine CC and blank data.

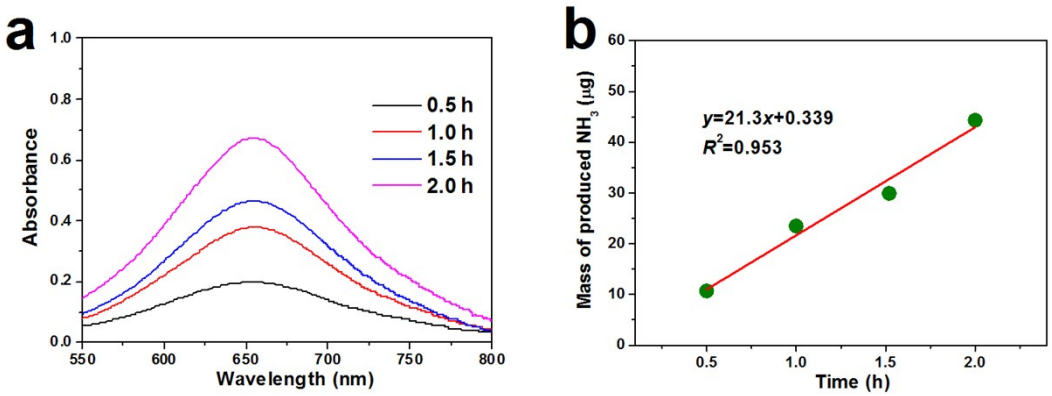

Fig. S9. (a) UV-Vis absorption spectra of the electrolytes after electrolysis at various times on Mo-SnS_2/CC at -0.5 V, and (b) corresponding mass of produced NH_3.

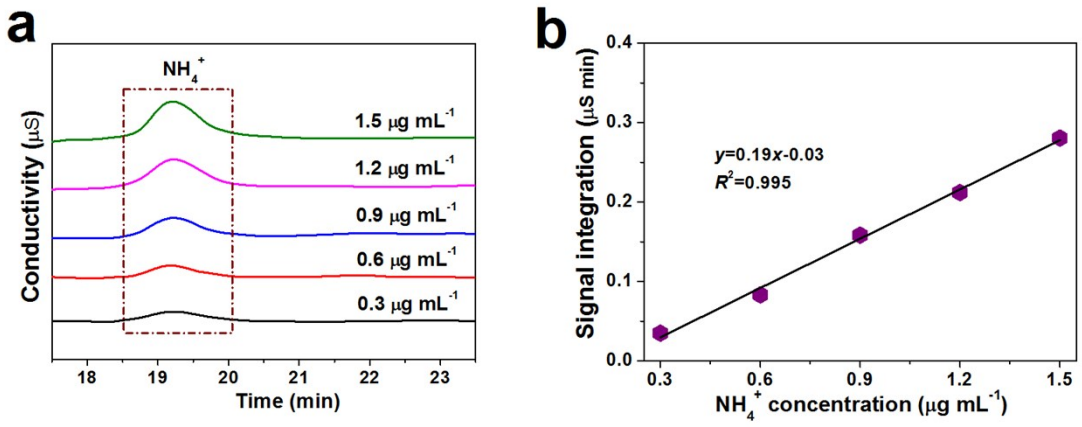

Fig. S10. (a) Ion chromatogram (IC) analysis of the NH_4^+ ions at different concentrations (inset), and (b) corresponding calibration curve of NH_4^+ concentration V_s. peak area.

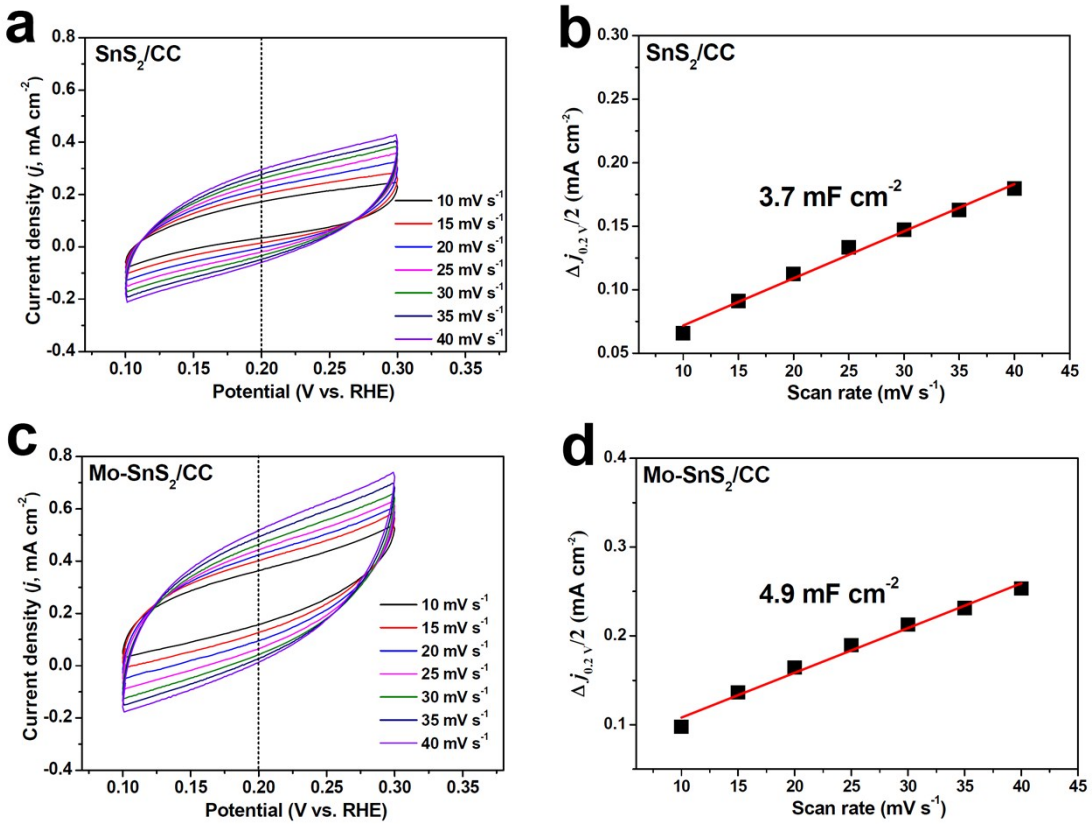

Fig. S11. Electrochemical double-layer capacitance (C_{dl}) measurements at different scanning rates of 10~40 mV s^{-1} for (a, b) SnS_2/CC and (c, d) Mo-SnS_2/CC.

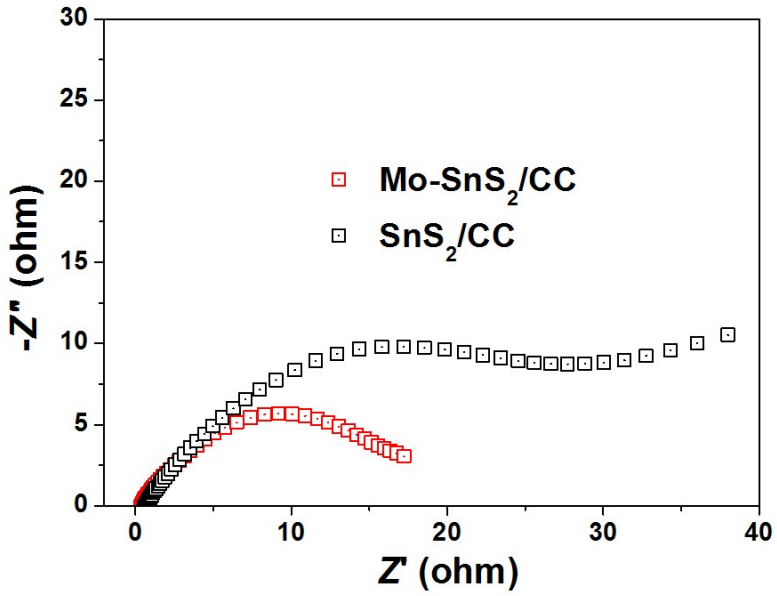

Fig. S12. Electrochemical impendence spectra of SnS_2/CC and Mo-SnS_2/CC.

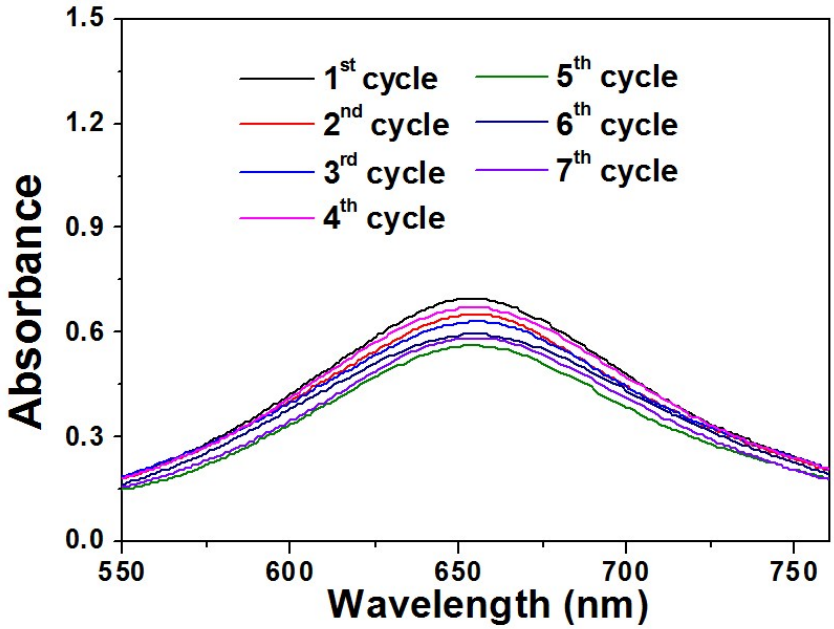

Fig. S13. UV-Vis absorption spectra of working electrolytes on Mo-SnS_2/CC (each for 2 h electrolysis at -0.5 V) for seven cycles.

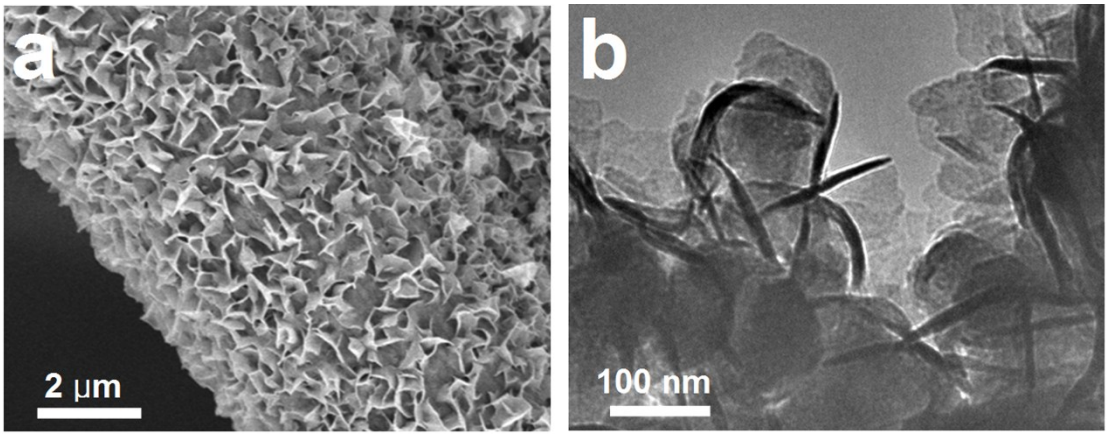

Fig. S14. Morphology of Mo-SnS_2/CC after stability test. (a) SEM. (b) TEM.

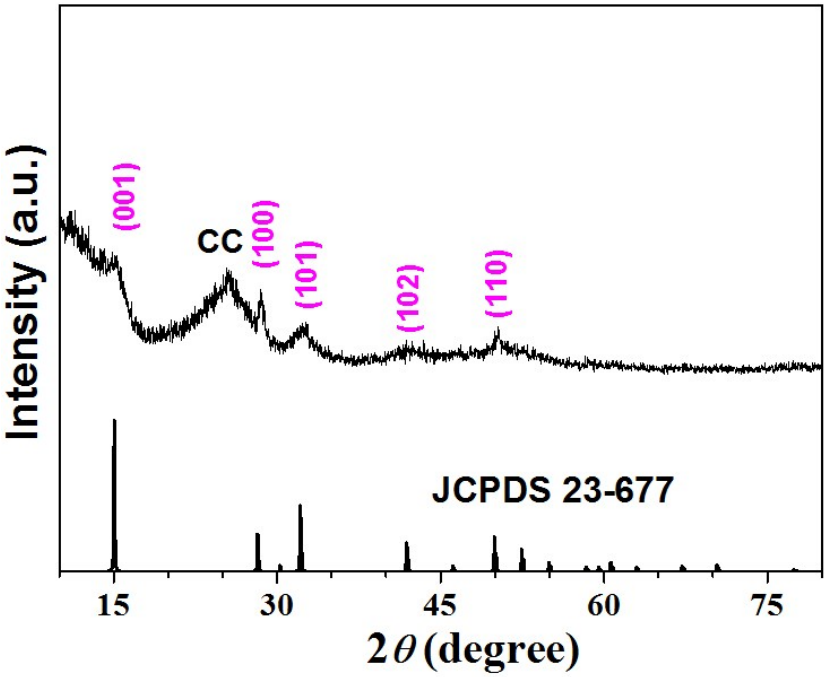

Fig. S15. XRD pattern of Mo-SnS_2/CC after stability test.

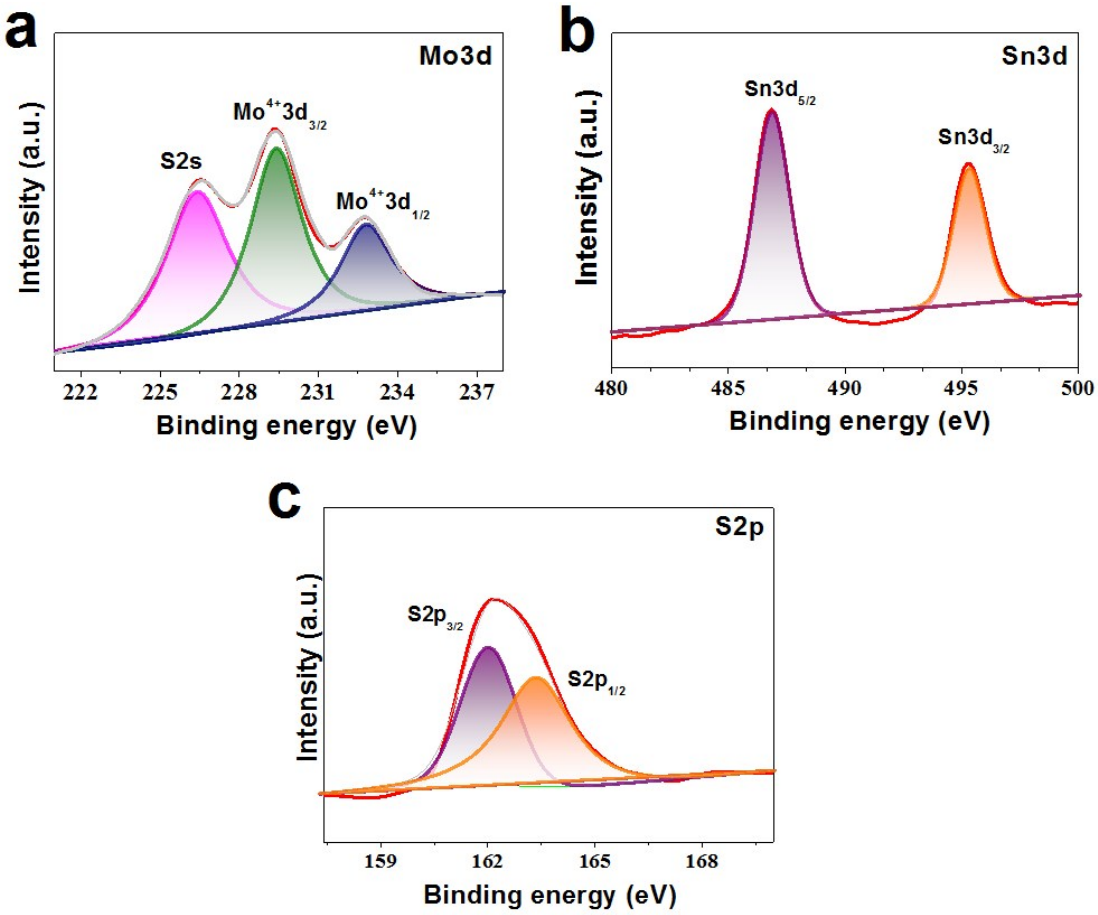

Fig. S16. XPS spectra of Mo-SnS_2 nanosheets scraped down from CC after stability test: (a) Mo3d; (b) Sn3d; (c) S2p.

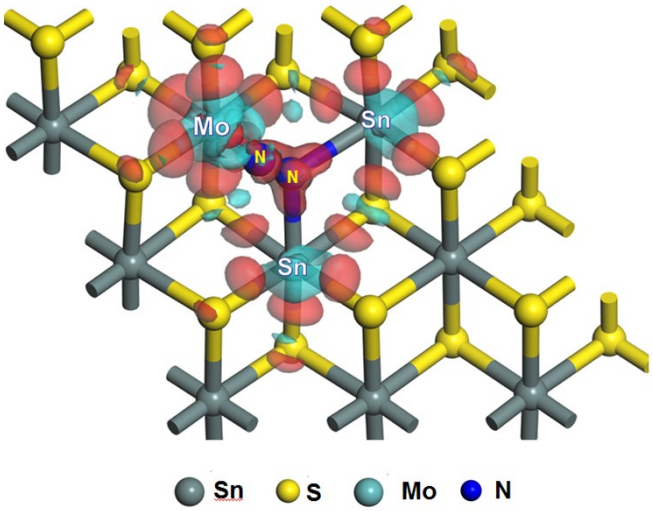

Fig. S17. Differential charge densities of Mo-Sn-Sn trimer after N_2 adsorption. Red and cyan regions correspond to the electron accumulation and depletion, respectively.

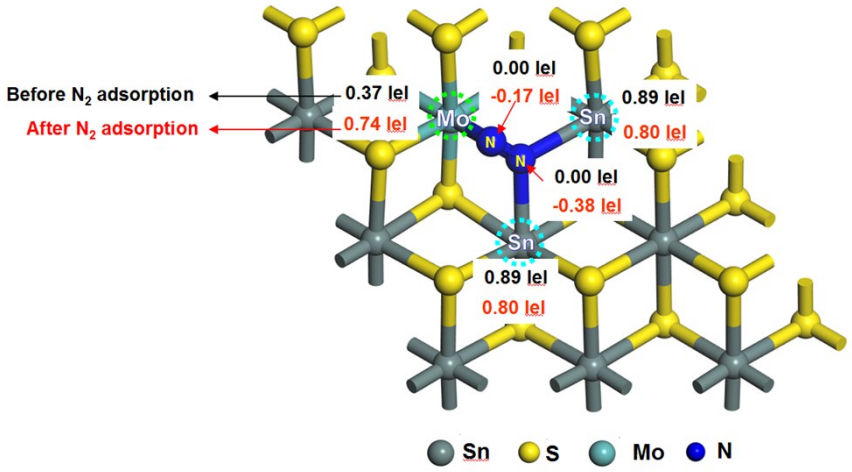

Fig. S18. Mulliken charge analysis of Mo-Sn-Sn trimer before (black) and after (red) N_2 adsorption.

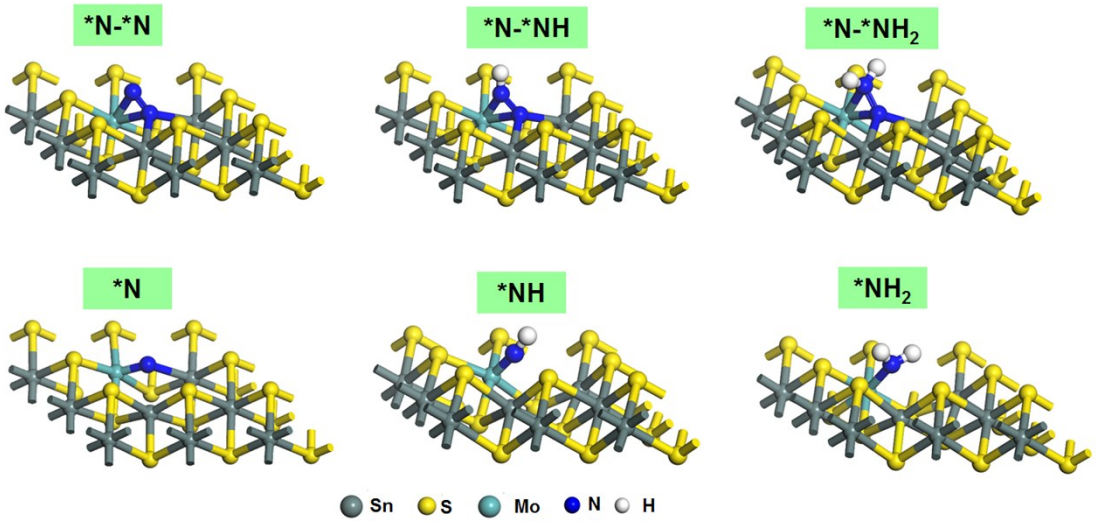

Fig. S19. Optimized structures of consecutive NRR intermediates over Mo-SnS_2-V_s.

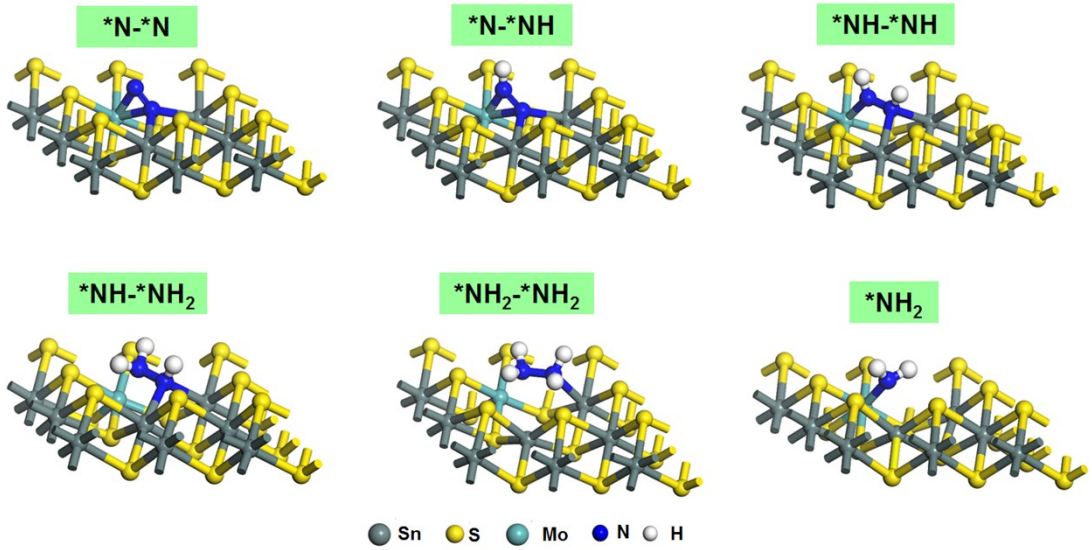

Fig. S20. Optimized structures of enzymatic NRR intermediates over Mo-SnS_2-V_s.

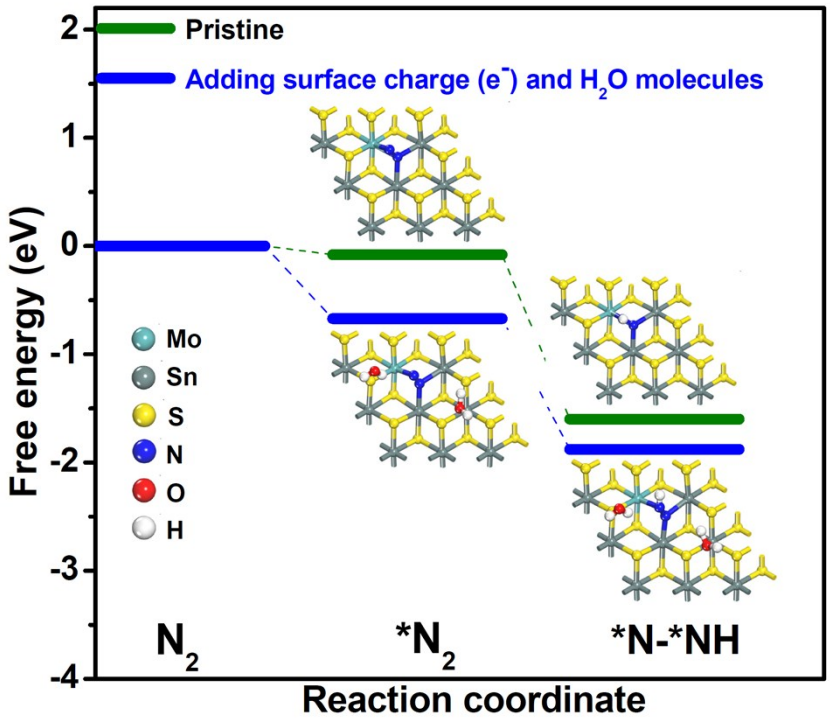

Fig. S21. Free energy diagrams of $*N_2$ and *N-*NH adsorption on Mo-SnS_2-V_s with (pristine) and without considering the effects of surface charge (adding one charge e^-) and hydrogen bonding (adding two H_2O molecules).

Table S1. Comparison of optimum NH_3 yield and Faradic efficiency (FE) for recently reported state-of-the-art NRR electrocatalysts at ambient conditions

Catalyst	Electrolyte	Determination method	Optimum Potential (V Vs RHE)	NH_3 yield rate	FE (%)	Ref.
Black phosphorus	0.01 M HCl	Indophenol blue method	-0.7	31.37 $\mu g\ h^{-1}\ mg^{-1}$	5.07 (-0.6)	[4]
MoO_2/graphene	0.1 M Na_2SO_4	Indophenol blue method	-0.35	37.4 $\mu g\ h^{-1}\ mg^{-1}$	6.6	[5]
Fe_2O_3 nanorod	0.1 M Na_2SO_4	Indophenol blue method	-0.8	15.9 $\mu g\ h^{-1}\ mg^{-1}$	0.94	[6]
Fe/Fe_3O_4	0.1 M PBS	Indophenol blue method	-0.3	0.19 $\mu g\ cm^{-2}\ h^{-1}$	8.29	[7]
S-doped carbon nanospheres	0.1 M Na_2SO_4	Indophenol blue method	-0.7	19.07 $\mu g\ h^{-1}\ mg^{-1}$	7.47	[8]
N-doped porous carbon	0.05 M H_2SO_4	Nessler's reagent method	-0.9	1.4 $mmol\ g^{-1}\ h^{-1}$	1.42	[9]
N-doped porous carbon	1.0 M HCl	Indophenol blue method	-0.3	9 $\mu g\ cm^{-2}\ h^{-1}$	5.2	[10]
Defective rich C_3N_4	0.1 M HCl	Indophenol blue method	-0.2	8.09 $\mu g\ h^{-1}\ mg^{-1}$	11.59	[11]
B-doped graphene	0.05 M H_2SO_4	Indophenol blue method	-0.5	9.8 $\mu g\ cm^{-2}\ h^{-1}$	10.8	[12]
Sulfur dots-graphene nanohybrid	0.5 M $LiClO_4$	Indophenol blue method	-0.85	28.56 $\mu g\ h^{-1}\ mg^{-1}$	7.07	[13]
Sulfur-doped graphene	0.1 M HCl	Indophenol blue method	-0.6	27.3 $\mu g\ h^{-1}\ mg^{-1}$	11.5 (-0.5V)	[14]
Cr_2O_3/RGO	0.1 M HCl	Indophenol blue method	-0.6	33.3 $\mu g\ h^{-1}\ mg^{-1}$	7.33	[15]
Boron-doped TiO_2	0.1 M Na_2SO_4	Indophenol blue method	-0.8	14.4 $\mu g\ h^{-1}\ mg^{-1}$	3.4	[16]
La_2O_3 nanoplate	0.1 M Na_2SO_4	Indophenol blue method	-0.8	17.04 $\mu g\ h^{-1}\ mg^{-1}$	4.76	[17]
Y_2O_3 Nanosheet	0.1 M Na_2SO_4	Indophenol blue method	-0.9	1.06×10^{-10} $mol\ s^{-1}\ cm^{-2}$	2.53	[18]
Defective TiO_2	0.1 M HCl	Indophenol blue method	-0.15	1.24×10^{-10} $mol\ s^{-1}\ cm^{-2}$	9.17	[19]
B_4C nanosheet	0.1 M HCl	Indophenol blue method	-0.75	26.57 $\mu g\ h^{-1}\ mg^{-1}$	15.95	[20]
MoS_2 nanosheet	0.1 M	Indophenol blue	-0.5	8.08×10^{-11}	1.17	[21]

	Na_2SO_4	method		mol s^{-1} cm^{-2}		
Defect-rich MoS_2 nanoflower	0.1 M Na_2SO_4	Indophenol blue method	-0.4	29.28 μg h^{-1} mg^{-1}	8.34	[22]
Au-TiO_2 sub-nanocluster	0.1 M HCl	Indophenol blue method	-0.2	21.4 μg h^{-1} mg^{-1}	8.11	[23]
Au nanorods	0.1 M KOH	Nessler's reagent method	-0.2	1.65 μg cm^{-2} h^{-1}	4.02	[24]
Mo_2C/C	0.5 M Li_2SO_4	Nessler's reagent method	-0.3	11.3 μg h^{-1} mg^{-1}	7.8	[25]
MXene	0.5 M Li_2SO_4	Nessler's reagent method	-0.1	4.7 μg cm^{-2} h^{-1}	5.78	[26]
Mosaic Bi nanosheets	0.1 M Na_2SO_4	Indophenol blue method	-0.8	13.23 μg h^{-1} mg^{-1}	10.46	[27]
Fe–N/C hybrid	0.1 M KOH	Indophenol blue method	-0.2	34.83 μg h^{-1} mg^{-1}	9.28	[28]
α-Fe nanorods	[C4mpyr][eFAP]	Indophenol blue method	-0.23	2.35×10^{-11} mol s^{-1} cm^{-2}	32	[29]
Amorphous Sn/crystalline SnS_2 nanosheets	0.1 M PBS	Indophenol blue method	-0.8	23.8 μg h^{-1} mg^{-1}	6.5 (-0.7V)	[30]
SnS_2 nanoarray on Ni foam	0.1 M Na_2SO_4	Indophenol blue method	-0.5	9.3×10^{-10} mol s^{-1} cm^{-2}	11.2	[31]
Mo-SnS_2/CC	0.5 M $LiClO_4$	Indophenol blue method	-0.5	41.3 μg h^{-1} mg^{-1}	20.8 (-0.4V)	This work

Table S2. Calculated ZPE and TΔS energies of various NRR intermediates over Mo-SnS_2

	△ZPE (eV)	TΔS **(eV)**
*N-*N	0.22	0.09
*N-*NH	0.46	0.13
*NH-*NH	0.85	0.12
NH-NH_2	1.18	1.08
NH_2-NH_2	1.45	0.15
*NH_2	0.76	0.05
N-NH_2	0.83	0.15
*N	0.09	0.05
*NH	0.4	0.05
N_2	0.15	0.6
H_2	0.27	0.4
NH_3	0.89	0.74

Supplementary references

[1]. D. Zhu, L. Zhang, R. E. Ruther and R. J. Hamers, *Nat. Mater.*, 2013, **12**, 836.

[2]. G. W. Watt and J. D. Chrisp, *Anal. Chem.*, 1952, **24**, 2006-2008.

[3]. S. J. Clark, M. D. Segall, C. J. Pickard, P. J. Hasnip, M. I. J. Probert, K. Refson and M. C. Payne, *Z. Kristallogr.*, 2005, **220**, 567-570.

[4]. L. L. Zhang, L. X. Ding, G. F. Chen, X. F. Yang and H. H. Wang, *Angew. Chem. Int. Edit.*, 2019, **131**, 2638-2642.

[5]. J. Wang, Y. P. Liu, H. Zhang, D. J. Huang and K. Chu, *Catal. Sci. Technol.*, 2019, **9**, 4248-4254.

[6]. X. Xiang, Z. Wang, X. Shi, M. Fan and X. Sun, *ChemCatChem*, 2018, **10**, 4530-4535.

[7]. L. Hu, A. Khaniya, J. Wang, G. Chen, W. E. Kaden and X. Feng, *ACS Catal.*, 2018, **8**, 9312-9319.

[8]. L. Xia, X. Wu, Y. Wang, Z. Niu, Q. Liu, T. Li, X. Shi, A. M. Asiri and X. Sun, *Small Methods*, 2018, **3**, 1800251.

[9]. Y. Liu, Y. Su, X. Quan, X. Fan, S. Chen, H. Yu, H. Zhao, Y. Zhang and J. Zhao, *ACS Catal.*, 2018, **8**, 1186-1191.

[10]. H. Wang, L. Wang, Q. Wang, S. Ye, W. Sun, Y. Shao, Z. Jiang, Q. Qiao, Y. Zhu and P. Song, *Angew. Chem. Int. Edit.*, 2018, **57**, 12360-12364.

[11]. C. Lv, Y. Qian, C. Yan, Y. Ding, Y. Liu, G. Chen and G. Yu, *Angew. Chem. Int. Edit.*, 2018, **57**, 10246-10250.

[12]. X. Yu, P. Han, Z. Wei, L. Huang, Z. Gu, S. Peng, J. Ma and G. Zheng, *Joule*, 2018, **2**, 1610-1622.

[13]. H. Chen, X. Zhu, H. Huang, H. Wang, T. Wang, R. Zhao, H. Zheng, A. M. Asiri, Y. Luo and X. Sun, *Chem. Commun.*, 2019, **55**, 3152-3155.

[14]. L. Xia, J. Yang, H. Wang, R. Zhao, H. Chen, W. Fang, A. M. Asiri, F. Xie, G. Cui and X. Sun, *Chem. Commun.*, 2019, **55**, 3371-3374.

[15]. L. Xia, B. Li, Y. Zhang, R. Zhang, L. Ji, H. Chen, G. Cui, H. Zheng, X. Sun, F. Xie and Q. Liu, *Inorg. Chem.*, 2019, **58**, 2257-2260.

[16]. Y. Wang, K. Jia, Q. Pan, Y. Xu, Q. Liu, G. Cui, X.-D. Guo and X. Sun, *ACS Sustain. Chem. Eng.*, 2018.

[17]. B. Xu, Z. Liu, W. Qiu, Q. Liu, X. Sun, G. Cui, Y. Wu and X. Xiong, *Electrochim. Acta*, 2018, **298**, 106-111.

[18]. X. Li, L. Li, X. Ren, D. Wu, Y. Zhang, H. Ma, X. Sun, B. Du, Q. Wei and B. Li, *Ind. Eng. Chem. Res.*, 2018, **57**, 16622-16627.

[19]. L. Yang, T. Wu, R. Zhang, H. Zhou, L. Xia, X. Shi, H. Zheng, Y. Zhang and X. Sun, *Nanoscale*, 2019, **11**, 1555-1562.

[20]. W. Qiu, X.-Y. Xie, J. Qiu, W.-H. Fang, R. Liang, X. Ren, X. Ji, G. Cui, A. M. Asiri and G. Cui, *Nat. Commun.*, 2018, **9**, 3485.

[21]. L. Zhang, X. Ji, X. Ren, Y. Ma, X. Shi, Z. Tian, A. M. Asiri, L. Chen, B. Tang and X. Sun, *Adv. Mater.*, 2018, **30**, 1800191.

[22]. X. Li, T. Li, Y. Ma, Q. Wei, W. Qiu, H. Guo, X. Shi, P. Zhang, A. M. Asiri and L. Chen, *Adv. Energy. Mater.*, 2018, **8**, 1801357.

[23]. M. M. Shi, D. Bao, B. R. Wulan, Y. H. Li, Y. F. Zhang, J. M. Yan and Q. Jiang, *Adv. Mater.*, 2017, **29**, 1606550.

[24]. D. Bao, Q. Zhang, F. L. Meng, H. X. Zhong, M. M. Shi, Y. Zhang, J. M. Yan, Q. Jiang and X. B. Zhang, *Adv. Mater.*, 2017, **29**, 1604799.

[25]. H. Cheng, L. X. Ding, G. F. Chen, L. Zhang, J. Xue and H. Wang, *Adv. Mater.*, 2018, **30**, 1803694.

[26]. Y. R. Luo, G. F. Chen, L. Ding, X. Z. Chen, L. X. Ding and H. H. Wang, *Joule*, 2019, **3**, 279-289.

[27]. L. Li, C. Tang, B. Xia, H. Jin, Y. Zheng and S.-Z. Qiao, *ACS Catal.*, 2019, **9**, 2902-2908.

[28]. Y. Wang, X. Cui, J. Zhao, G. Jia, L. Gu, Q. Zhang, L. Meng, Z. Shi, L. Zheng and C. Wang, *ACS Catal.*, 2018, **9**, 336-344.

[29]. B. H. Suryanto, C. S. Kang, D. Wang, C. Xiao, F. Zhou, L. M. Azofra, L. Cavallo, X. Zhang and D. R. MacFarlane, *ACS Energy Lett.*, 2018, **3**, 1219-1224.

[30]. P. Li, W. Fu, P. Zhuang, Y. Cao, C. Tang, A. B. Watson, P. Dong, J. Shen and M. Ye, *Small*, 2019, **15**, 1902535.

[31]. X. Chen, Y.-T. Liu, C. Ma, J. Yu and B. Ding, *J. Mater. Chem. A*, 2019, **7**, 22235-22241.